DOI: 10.13009/EUCASS2023-562
Aerospace Europe Conference 2023 – 10TH EUCASS – 9TH CEAS

Resistive MHD simulations of a self-field magneto-plasmadynamic thruster over the 5 to 40 kA current range

Yevhen Tkachenko[⋆†], *Andrea Ciardi*[⋆] *and Benjamin Khiar*[⋆⋆]
[⋆]*Sorbonne Université, Observatoire de Paris, PSL Research University, LERMA, CNRS UMR 8112*
4 place Jussieu 75005 Paris, France
[⋆⋆]*DPHY, ONERA, Université Paris Saclay*
6 Chemin de la Vauve aux Granges F-91123 Palaiseau, France
yevhen.tkachenko@obspm.fr · andrea.ciardi@obspm.fr · benjamin.khiar@onera.fr
[†]Corresponding author

Abstract
Self-field magnetoplasmadynamic thrusters (MPDTs) are a promising class of electric space propulsion (EP) devices. The acceleration of the plasma propellant in MPDTs is mostly done by the Lorentz force produced by the interaction of the discharge current and the induced (self) magnetic field. Despite its unique ability among EP devices to efficiently handle very high power levels with a relatively simple design, the wide spread use of self-field MPDTs is limited, in addition to the currently unavailable high power sources, by the "onset": an unstable plasma behaviour that is experimentally observed for currents above a critical current.

In this paper we investigate numerically the plasma dynamics of argon self-field MPDTs over a wide range of currents ($J = 5 - 40$ kA) including super-critical ones ($J_c \approx 17$ kA). We perform single-fluid, two temperature, resistive magnetohydrodynamic (MHD) simulations in 2D cylindrical axisymmetric geometry. The simulations recover the expected values of the thrust for the two known operational regimes of MPDTs, with the acceleration of the plasma being pressure-driven at low currents and magnetically-driven at high currents. The power at high currents follows the expected scaling $\sim J^4$. We find that while the physical model employed recovers well the expected dynamics of MPDTs, for currents above the critical current J_c the simulations show instead stable plasma behaviour. The results indicate that to trigger the "onset", simulations will need to include more physical processes, as well as being extended to three-dimensions.

1. Introduction

Magnetoplasmadynamic thrusters (MPDTs) are promising devices in the electric space propulsion (EP) family where acceleration is mostly done by the Lorentz force. While MPDTs share the ability of all EP devices to achieve large exhaust velocities, u_{ex}, and provide improved payload capacity, they also have some unique features. For example, they exhibit not only high specific impulses, but also high values of thrust with very interesting thrust densities up to 50 N m^{-2} (Ahedo 2011; Mazouffre 2016; Sutton et al. 2016). While showing high efficiency of electric to kinetic energy conversion, they are easier to design than other EP devices and they are known to have simple scalability of thrust with current at high powers, (Ahedo 2011; Sutton et al. 2016). It has been shown analytically (see Maecker 1955; Jahn et al. 1968) that the thrust produced by MPDTs is dependent on the square of the driving current

$$T = \frac{\mu_0 J^2}{4\pi}\left(ln\frac{r_a}{r_c} + A\right) = \frac{\mu_0 J^2}{4\pi} C_T J^2 \tag{1}$$

where T is thrust, J is the total current driving the MPDT system, r_c - the cathode radius, r_a - the anode radius, μ_0 - the vacuum permeability. The constant of the order of unity, A, indicates how the shape of the cathode tip affects the overall thrust. Maecker's formula clearly shows that the only thrust dependency on the geometry of an MPDT is coming from the anode to cathode radii ratio and the cathode tip's shape. Both these dependencies are encapsulated in the dimensionless thrust coefficient parameter C_T. Both constants A and C_T will be discussed later in the paper.

While the dependency expressed in Eq. 1 has been successfully confirmed by several experiments performed at relatively high currents, it was also shown to fail at relatively low currents, (see Choueiri 1998; Sankaran et al.

DOI: 10.13009/EUCASS2023-562

2005; Andrenucci 2010) and a review by (Ahedo 2011). In case of a mass flow rate of 6 g s^{-1}, and for currents below $\sim 12-13$ kA MPDTs rather works similarly to arcjets, where the current essentially heats the propellant allowing it to expand at relatively moderate velocities. Above these currents MPDTs become more efficient as the Lorentz force dominates the acceleration. Since in this regime of high efficiency an MPDT requires more current and therefore more power it is usually called the high-current or high-power regime of an MPDT.

At even higher currents, $J \gtrsim 17.5$ kA, the so-called "onset" occurs (see Boyle et al. 1976; Choueiri et al. 1987; Uribarri et al. 2005; Uribarri 2008; Andrenucci 2010), which is characterised by severe anode erosion, voltage oscillations and loss of efficiency. Since MPDTs are difficult to study analytically and despite many theoretical and experimental studies, summarized in Andrenucci 2010, the cause of this breakdown remains unclear.

Furthermore, experiments in high-power regimes are challenging because of high pumping requirements in vacuum chambers, as well as difficulties in providing an adequate power supply, in particular for steady-state MPDTs. As a result, notable efforts have been aimed at the numerical investigation of MPDTs. Sankaran et al. 2005 studied MPDT dynamics in the subcritical or near-critical current regimes. In particular the authors used inlet boundary conditions designed to achieve high ionisations consistent with experiments. Their simulations also showed that plasma in the near-anode region may experience depletion of electrons with increasing current, possibly contributing to the onset appearance. Later Kawasaki et al. 2014; Kawasaki et al. 2015 estimated the role of thermal phenomena as a possible reason of the MPDT anode's melting. The simulations exhibited regions where anode temperature reaches slightly higher values. Also the possible impact of the cathode radius and its root temperature on the anode temperature was investigated among other things. While the onset remains unexplained, some MHD studies focus on estimations of the MPDT efficiency (Xisto et al. 2015) and/or on the numerical investigation of applied-field MPDTs (Chelem Mayigué et al. 2018), which are known to have higher stability than self-field MPDTs. In addition to MHD modelling, PIC simulations have also been used to study applied-field MPDTs (see Tang et al. 2012).

The aim of the present numerical work is to investigate the physics of self-field MPDTs over a range of currents including the high-current regime where the onset is thought to occur. However we do not expect to capture the onset here as existing 2D axisymmetric cylindrical MHD simulations indicate that the physics included and the axisymmetric geometry may not be sufficient. This work is intended to build the numerical tools and physical models that are needed in order to correctly study the MPDT dynamics, and to lay the foundations to conduct future studies including more complex processes that could be responsible for the onset.

In the framework of the present work we run single-fluid, two temperature, resistive magnetohydrodynamic (MHD) simulations in 2D cylindrical axisymmetric geometry using the publicly available, massively parallel, finite-volume code FLASH (Fryxell et al. 2000). In the following section the numerical model and the FLASH code will be presented. Then a standard case at 15 kA current will be described. Comparisons with expected theoretical and experimental thrust levels will be given and finally a discussion about the energy budget will be conducted.

2. MPDT basics and Numerical Method

A typical MPDT, see Fig. 1, is a compact axisymmetric electric device in which a propellant is fed between two coaxial electrodes, see Fig. As breakdown of the gas is initiated, an electric current flows from one electrode to another through the plasma resulting in acceleration of the latter. The acceleration in an MPDT is generated by a combination of the Lorentz and the thermal pressure gradient forces. These thrusters are unique in that they can easily operate efficiently at very high power levels, typically several hundreds of kilowatts. At relatively low current levels (a few kA maximum), MPDT behave basically as arcjets with most of the thrust produced by hydrodynamical expansion of the joule-heated propellant. As current (and power) is increased, Lorentz forces dominate the acceleration process and high efficiency can be achieved.

Since the presence of geometrical peculiarities in the MPDT geometry may affect the physics of plasma acceleration, we focus this work on a simple design. Namely, the geometry of MPDT is chosen to follow the Villani benchmark setup (see Villani 1982) where electrodes are coaxial and their lengths and radii have the following values: $r_c = 0.95\ cm$, $r_a = 5.1\ cm$, $l_c = 26.4\ cm$, $l_a = 20.0\ cm$. The anode to cathode radii ratio is an important geometrical similarity parameter in Maecker's formula. Keeping it ~ 5.37 allows our results to be comparable with multiple experiments as the same radii ratio or very close to it is used among various experimental (Boyle et al. 1976; Villani 1982; Sankaran et al. 2005) and numerical (Auweter-Kurtz et al. 1989; Sankaran et al. 2005; Sankaran 2005; Kawasaki et al. 2014) setups, to name a few. The inter-electrode cross-section is kept constant in order to investigate the Lorentz force acceleration and also to avoid additional components of thrust due to an expanding nozzle.

DOI: 10.13009/EUCASS2023-562

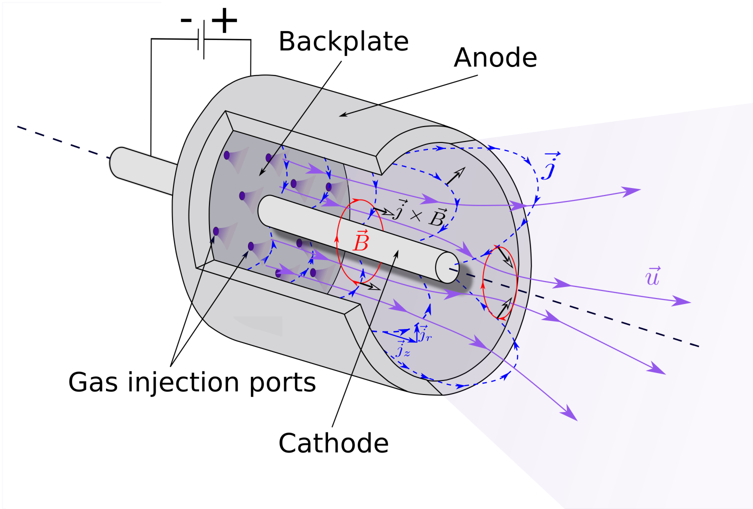

Figure 1: MPDT schematics in 3D. MPDT consists of an anode, a cathode, a power supply and a backplate with propellant injection ports. The electric current $\vec{j} = (j_r, 0, j_z)$ (blue dashed lines) and its induced magnetic field $\vec{B} = (0, B_\theta, 0)$ (red solid lines) together produce the Lorentz force (black arrows). It accelerates ionised propellant (purple) in both axial, by $j_r B_\theta$, and radial, by $j_z B_\theta$, directions. The approximate streamlines of velocity $\mathbf{u}$ are shown with violet solid lines. The black dashed line represents the axis of symmetry.

2.1 The FLASH resistive MHD code

2D cylindrical axisymmetric simulations are performed with the FLASH code (Fryxell et al. 2000): a massively parallel, finite-volume eulerican code that solves the single-fluid, two-temperatures resistive magnetohydrodynamic equations: the continuity equation, Eq. 2, the conservation of momentum equation, Eq. 3, the conservation of ion, Eq. 4, and electron, Eq. 5, internal energies equations as well as the induction equation, Eq. 6. It should be noted that for numerical reasons and difficulties arising from estimating $\nabla \cdot \mathbf{u}$ at shocks, FLASH partially solves Eq. 4 and 5 and additionally solves the conservation equation for total energy in order to compute indirectly the pressure work terms using the so-called RAGE-like approach, see *FLASH user's guide*.

$$\frac{\partial \rho}{\partial t} + \nabla \cdot (\rho \vec{u}) = 0 \tag{2}$$

$$\frac{\partial \rho \vec{u}}{\partial t} + \nabla \cdot (\rho \vec{u} \vec{u}) = -\nabla (p_e + p_i) + \vec{j} \times \vec{B} \tag{3}$$

$$\frac{\partial \varepsilon_e}{\partial t} + \nabla \cdot (\varepsilon_e \vec{u}) = -p_e \nabla \cdot \vec{u} - \nabla \cdot \vec{q}_e + \eta j^2 - Q_{ei} \tag{4}$$

$$\frac{\partial \varepsilon_i}{\partial t} + \nabla \cdot (\varepsilon_i \vec{u}) = -p_i \nabla \cdot \vec{u} - \nabla \cdot \vec{q}_i + Q_{ei} \tag{5}$$

$$\frac{\partial \vec{B}}{\partial t} = \nabla \times (\vec{u} \times \vec{B}) - \nabla \times (\eta \vec{j}) \tag{6}$$

where ρ is the mass density, $\mathbf{u}$ is the fluid velocity, $p_{e/i} = n_{e/i}\, k_B\, T_{e/i}$ are electron and ion pressures respectively, ε_e and ε_i are electron and ion internal energy densities, $q_{e/i} = -\kappa_{e/i} \nabla T_{e/i}$ - the electron/ion heat fluxes, $Q_{ei} = -3 \frac{m_e}{m_i} n_e \nu_{ei} k_B (T_e - T_i)$ - the heat exchange rate due to electron-ion collisions and η is the electric resistivity. Electric current density $\mathbf{j}$ taking place in the ohmic heating term, ηj^2, and the magnetic diffusion term in the induction equation, Eq. 5, is derived from the magnetic field $\mathbf{B}$ thanks to the Ampere's law $\vec{j} = \frac{1}{\mu_0} \nabla \times \vec{B}$. The simulations include Braginskii transport coefficients (Braginskii 1965), as well as a tabulated EOS calculated with the IONMIX code (Macfarlane 1989). Radiation transport is not included in our modelling. Simulations were run with the second-order HLLC scheme, implicit thermal conduction and explicit resistive diffusion (see *FLASH user's guide*, for the details of the implementation).

DOI: 10.13009/EUCASS2023-562

2.2 Boundary conditions

The geometric configuration of the Villani MPDT setup is depicted in Figure 2a. It comprises two coaxial cylindrical electrodes with varying heights. The z axis is the axis of symmetry. The electrodes are represented by black rectangles. The one aligned to the axis of symmetry is the cathode and below is the anode. The injection of the plasma takes place at $z = 0$, between the electrodes in the region $r_c < r < r_a$ (left hand side of the image). All simulations are run with a mass flow rate $\dot{m} = 6\ \mathrm{g\,s^{-1}}$. The use of this specific mass flow rate allow us to compare the simulation results with available experimental data. The propellant is injected with a uniform inlet velocity, density, pressure, and with a magnetic field $B \sim 1/r$. The inlet is injected at supersonic speed with Mach number of $M \approx 1.4$.

Experimental measurements by Randolph et al. 1992 suggest that the gaseous propellant rapidly becomes fully-ionised. The ratio of the ion to neutral number densities reaches 10 just downstream of the inlet. In Sankaran 2001; Sankaran et al. 2005 the plasma was injected with a temperature of $\sim 1.0 - 1.3$ eV corresponding to an effective ionisation $\bar{Z} = 1$. Similarly we initialise the plasma at the inlet with a temperature of 1.3 eV. However, we find that both IONMIX (Macfarlane 1989) and FLYCHK (Chung et al. 2003, 2005) calculations give lower effective ionisations. Therefore in our work we allow the plasma to be injected with a $\bar{Z} = 0.2$. We will see later that the plasma is rapidly ionised downstream of the inlet, however regions of low ionisation still persist indicating the need to include electron-neutral collisions in the calculation of the resistivity. This work is in progress.

The other two boundaries, $r = 10.2$ cm and $z = 51.0$ cm, are the outflow boundaries. While plasma is allowed to freely pass through these boundaries, magnetic field on the other hand is chosen to be zero. This way all the current is confined to the computational domain. The boundaries are carefully located far downstream so they do not affect the magnetic field distribution in the MPDT system. We note that such boundaries do not allow any current attachments on the anode's outer surface, since it is not in the computational domain. However, as it has been shown by Choueiri 1998, these current attachments are not essential for the total thrust calculation.

In the FLASH code, the plasma-electrode interfaces play the role of "in-domain" boundaries with adiabatic conditions. At the same time they provide reflection boundaries for the flow. Within the framework of this work the code has been extended to allow magnetic field diffusion into the electrodes. After magnetic field diffuses into the electrodes, the plasma flow achieves steady-state. With this functionality being included in the FLASH simulations, magnetic field and current distributions show better agreement with the corresponding experimental measurements of Sankaran et al. 2005; Sankaran 2005. Also, magnetic field in the cathode is proportional to the radial distance, $B \sim r$ as it follows from the Ampere law. No other boundary conditions were added to keep linear dependency of magnetic field in the electrodes. The resistivity of the electrodes is chosen to be the one of copper, $\eta = 1.68 \times 10^{-8}\ \Omega$ m , as the latter is frequently used as MPDT's electrodes material.

3. General dynamics and scaling with current

We now present in detail the simulation results for the reference current of $J = 15.0$ kA. At this current and mass flow rate an MPDT is in the high-power regime. Fig. 2 shows the spatial distributions of the plasma parameters in steady-state operation. The only component of the magnetic field in this self-field MPDT is the azimuthal component, and its distribution is shown in Fig. 2a. The magnetic field is strongest close to the cathode and falls with the axial distance. Given that only the azimuthal component of the magnetic field is present, the Lorentz force vector is always in the $r - z$ plane of Fig. 2a and its direction can be easily found as perpendicular to the current streamlines shown. The Lorentz force accelerating the plasma in the axial direction is largest close to the cathode, and this corresponds to the rapid increase in the velocity (Fig. 2b) in this region. The propellant is injected with an axial velocity $u \sim 3.0 \times 10^3$ m/s and reaches velocities $u \sim 3.5 \times 10^4$ m/s close to the axis at the outlet (the right hand side outflow boundary $z = 51$ cm).

As propellant accelerates it becomes rarefied, see Fig. 2c. In addition to the axial acceleration, the plasma is pushed towards the cathode not far downstream from the inlet by the magnetic "pinching" force. This leads to a compression of the plasma, as seen in the increase electron and ion densities, as well as temperatures. This density enhancement was also observed in the simulations by Sankaran et al. 2005. However, we find that the choice of the EOS can greatly affect the distribution of the ion number density. For example, when using a constant ionisation of $\bar{Z} = 1$, we observe an electron density distribution similar to that of Sankaran et al. 2005. In the case of a more realistic EOS and ionisations, calculated with the IONMIX code, the impact on the resistivity, and thus the diffusion and advection of magnetic field, is such that the magnetic "pinching" force becomes insufficient to maintain enhanced ion number density close to the cathode further downstream.

Close to the cathode the argon plasma quickly becomes fully ionised, see Fig. 2e. Few millimetres downstream the mean ionisation levels at the cathode face are found to be ~ 3. At the larger radii however the ohmic heating is not sufficient to fully ionise the plasma and the ionisation level remains below 1.

DOI: 10.13009/EUCASS2023-562

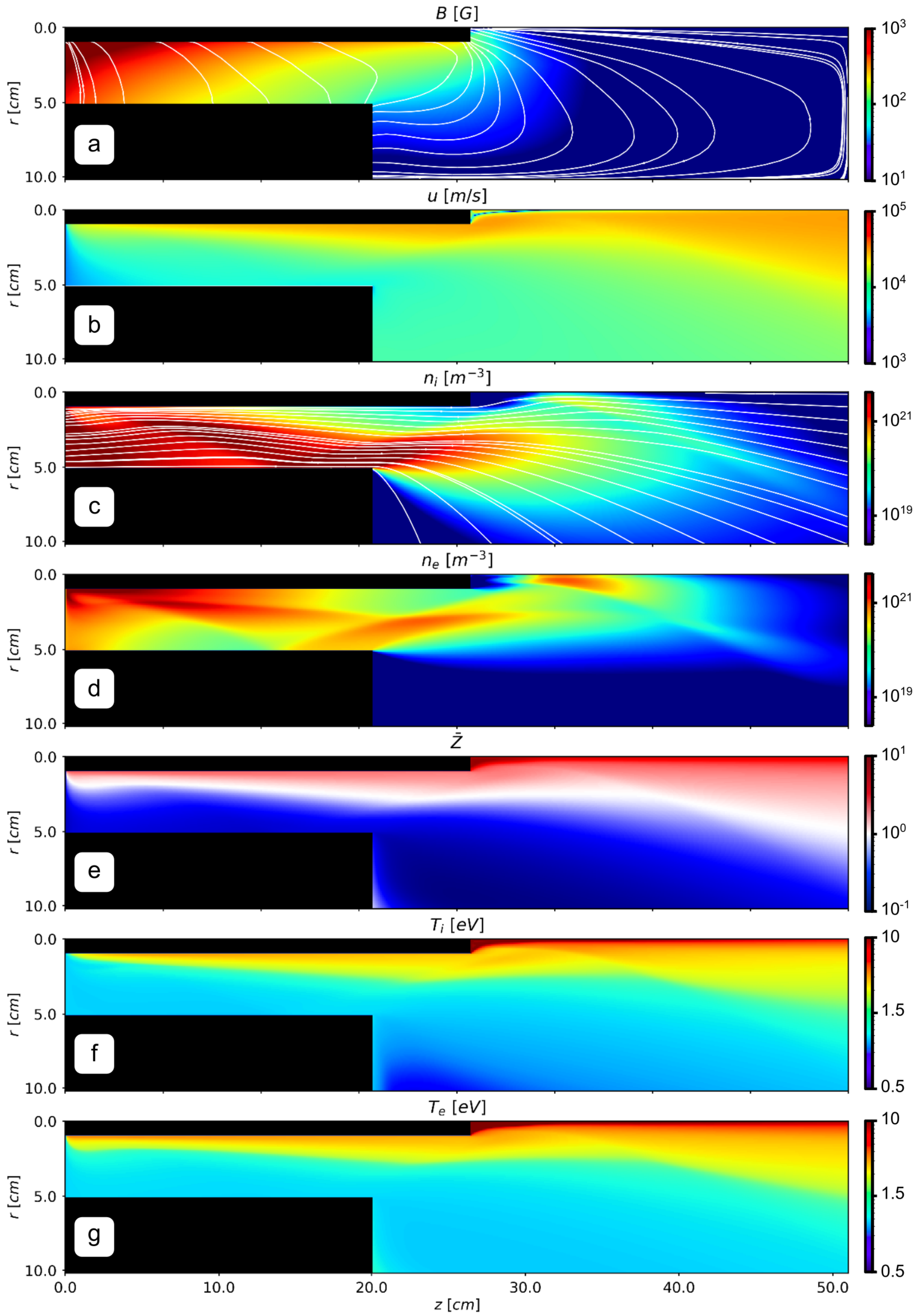

Figure 2: Spatial distribution of flow parameters in the Villani MPDT setup for the case $J = 15$ kA, $\dot{m} = 6$ g s^{-1}. The black rectangles represent the electrodes. Panel (a) shows the magnetic field magnitude in G (colour map) and the current streamlines (white lines); panel (b) - the magnitude of the flow velocity in m/s; panel (c) - the ion number density in m^{-3} (colour map) and the velocity streamlines (white lines); panel (d) - the electron number density in m^{-3}; panel (e) - the effective ionisation level; panels (f) and (g) - the ion and electron temperatures respectively in eV.

DOI: 10.13009/EUCASS2023-562

We note that in these regions the resistivity is underestimated, Spitzer resistivity is no longer valid and electron-neutral collisions should also be taken into account, as shown for example in the simulations with the Mach2 code by LaPointe et al. 2001 of hydrogen-fed MPDT. The implementation of a resistivity module including electron-neutral collisions is in progress.

Equilibration time is short enough so ion and electron temperatures are almost the same throughout the simulation box, see temperature distributions in Fig. 2f and 2g.

The ohmic heating is higher close to the cathode and therefore the temperature of the electrons is higher in that region. Increasing from ~ 1.3 eV at the inlet boundary to ~ 5 eV at the cathode surface not far from the inlet.

At the cathode tip the magnetic field pinches the propellant radially inward. The corresponding thermal pressure enhancement leads to the appearance of an additional thrust component as plasma pushes on the cathode tip. Here plasma is rarefied and both electron and ion temperatures become much higher reaching $\sim$10 eV. Ionisation level in this region is found to be around 6.

The simulations successfully reproduce the values of thrust found in experiments conducted by Choueiri 1998 and Sankaran et al. 2005 for a slightly different geometrical setup, called the Princeton Full-Scale Benchmark Thruster, or PFSBT. MPDT results are usually compared in terms of the so-called thrust coefficient C_T, which, using Maeker's formula, Eq. 1, is given by

$$C_T = \frac{4\pi}{\mu_0}\frac{T}{J^2} \tag{7}$$

$$= \left(ln\frac{r_a}{r_c} + A\right) \tag{8}$$

The thrust coefficient C_T is constant and its value is determined by the MPDT geometry. For example, in case of the Villani MPDT setup with the truncated cathode tip the geometrical paremeter A is $1/4$, while for the PFSBT it is $3/4$ due to the conic shape of the cathode tip. Both setups share the same value of $r_a/r_c \sim 5.37$, but due to the different values of A the expected C_T are therefore different: 1.93 and 2.43 in case of the Villani and PFSBT setups respectively. Thus for the same current levels J one expects different thrusts T to be produced by the two setups.

Fig. 3 shows the thrust coefficient C_T as a function of current calculated from the simulations, as well as theoretical relations found by Maecker 1955; Jahn et al. 1968; Tikhonov et al. 1993 and experimental data by Choueiri 1998; Sankaran et al. 2005. The simulation results reproduce both analytical predictions and experimental value of thrust levels for both low- and high-current regimes. Maecker's formula is experimentally proven to be valid for high-current regime only (Choueiri 1998). In this regime the simulation results, marked with red dots, in case of the Villani MPDT setup closely follow Maecker's formula, marked with dashed red line. At the same time experimental data by Choueiri 1998 and Sankaran et al. 2005, marked with blue pluses and black crosses in Fig. 3 respectively, have slight deviation from their characteristic C_T value of 2.43, marked with black dashed line. This is due to peculiarities of the anode geometry of the PFSBT setup. The accompanying simulations performed by Sankaran et al. 2005 with their own code (Sankaran et al. 2001), for the PFSBT setup indicate good agreement with experiments, see the black dots in Fig. 3.

The simulations by Sankaran et al. 2005 were however limited to the high-current subcritical regime. In the present work we extended the current range to both low and supercritical currents. At low currents Maecker's formula is known to fail and the relation found by Tikhonov et al. 1993 must be used instead. The latter work investigated an MPDT in a 1.5-dimension approximation with plasma *beta* being 1 at the inlet and enclosed current, as well as magnetic field magnitude, being zero at the outlet. The flow was assumed to be isothermal, single fluid, having single temperature and with high magnetic Reynolds number. The corresponding thrust coefficient relation found by Tikhonov et al. 1993 is

$$C_T = \left(\frac{\gamma+1}{2}\right) + \frac{1}{2}\left(\frac{\gamma\mu}{8\pi C_S}\frac{J^2}{\dot{m}}\right)^{-2} \tag{9}$$

where γ is the heat capacity ratio, C_S is the sound speed of the fully accelerated flow. This relation, marked with solid black line in Fig. 3, indicates that at low current the acceleration must be done by thermal pressure gradient. Our MPDT simulations are able to reproduce the pattern found by Tikhonov et al. 1993 for low currents.

However, it is the high-current regime which is of special interest as in this regime MPDTs have higher efficiency. Experimental findings have shown that when dealing with large currents, self-field MPDTs in the high-power regime are disrupted by the onset, characterized by current filamentation, anode erosion, and plasma instabilities (Boyle et al. 1976; Uribarri et al. 2005; Uribarri 2008; Andrenucci 2010). This occurs for currents above a critical value of the current which is approximately given by Choueiri et al. 1987, $J_c = \sqrt{k_* \dot{m}}$ kA, where $k_* \approx 40$ kA^2 s g^{-1}. For a mass flow rate of 6 g s^{-1} the threshold is $J_c \sim 15$ kA.

DOI: 10.13009/EUCASS2023-562

The simulations presented here indicate that when operating at high current levels (>20 kA) well above the expected critical current, the plasma flow is still steady-state. This indicates that the onset cannot be captured by the 2D axisymmetric, resistive MHD simulations employed here.

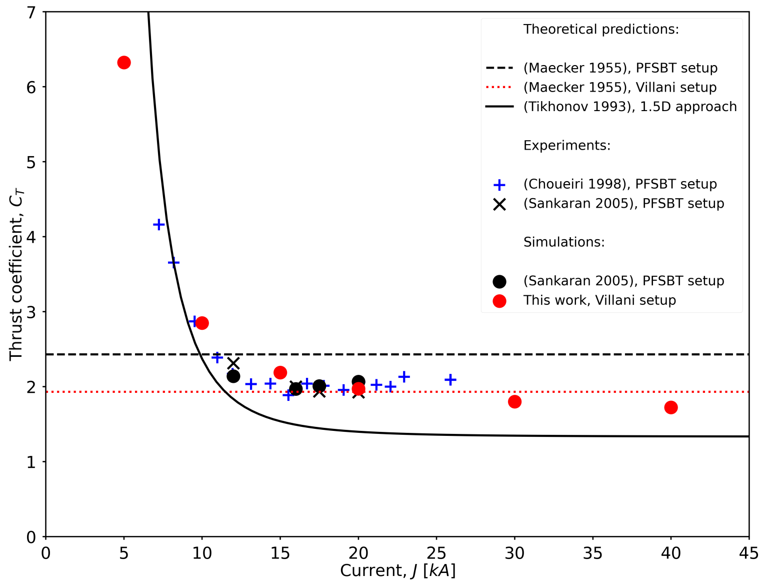

Figure 3: Thrust coefficient dependency on the total current. Simulation results show good agreement with Maecker's formula at high currents. At the same time they properly reproduce thrust levels as predicted by Tikhonov et al. 1993 at low currents. Thus FLASH simulations extend the range in which previous MHD simulations were done. Despite slight geometrical differences in the Villani and PFSBT setups the results are comparable when the cathode tip's shape is properly taken into account. FLASH MPDT simulations clearly indicate two operational regimes: the low-current regime where acceleration is mostly done by the thermal pressure gradient and the high-current regime - with the Lorentz force being the dominant one.

Thrust efficiency is central to the question of MPDTs operability. The total input power UJ (with U being the driving applied voltage between the two electrodes) is redistributed among acceleration, heating, ionisation and excitation. The acceleration power is simply the amount of axial kinetic energy produced by an MPDT per unit time, $P_T = \frac{\dot{m}\, u_{ex}^2}{2} = \frac{T^2}{2\dot{m}}$, there u_{ex} is the exhaust velocity. The thrust T here consists of three parts $T = T_c + \int\limits_V \left(\vec{j} \times \vec{B}\right)_z dV + \int\limits_V (\nabla p)_z\, dV$. Here $T_c = \dot{m} u_{in}$, the cold thrust, a thrust produced by the flow injected into MPDT chamber at u_{in} velocity. The second term is the thrust produced by the electromagnetic force and the third one is that due to the thermal pressure force. The power spent to electromagnetically accelerate the flow is $P_M = \int\limits_V \left(\vec{j} \times \vec{B}\right) \cdot \vec{u}\, dV$. Additionally, a noticeable amount of power is spent as ohmic heating since the MPDT argon plasma is characterised by a non-negligible resistivity η. The corresponding power is equal to $P_\eta = \int\limits_V \eta j^2\, dV$. Energy conservation implies that

$$UJ = P_M + P_\eta \tag{10}$$

Since the plasma injected in the simulations is assumed to be already partially ionised, the power spent in creating the initial hot plasma may be non-negligible in the low-current regime. We will see later that this power will therefore be included in the expression for the thrust efficiency apart from UJ.

The power spent to generate the inlet plasma is

$$\dot{\varepsilon}_{init} = \int\limits_S (\frac{1}{2} \rho\, u_{in}^2 + \rho\, \varepsilon_{int} + p) u_{in} dS \tag{11}$$

where ε_{int} is the specific internal energy of plasma, p is the total thermal pressure. The integration here is done over the inlet surface. The first term of Eq. 11 corresponds to the kinetic energy of the injected flow while other two together represent its enthalpy. In case of uniform injection conditions the above expression may be rewritten as $\dot{\varepsilon}_{init} = (1/2\, u_{in}^2 + \varepsilon_{int} + p/\rho)\dot{m}$. The specific internal energy includes translational (thermal), excitation and ionisation energies $\varepsilon_{int} = \varepsilon_{th} + \varepsilon_{ex} + \varepsilon_{ion}$.

DOI: 10.13009/EUCASS2023-562

The power associated with the kinetic energy of the inlet is also simply

$$\dot{\varepsilon}_k = \frac{T_c^2}{2\dot{m}} = \frac{\dot{m}u_{in}^2}{2} \tag{12}$$

The amount of thermal energy stored in the injected plasma is

$$\dot{\varepsilon}_{th} = \frac{3}{2}k(T_{ion} + \bar{Z}T_{ele})\frac{\dot{m}}{m_{Ar}} \tag{13}$$

where the average thermal energy of an ion and an electron at the given temperature is multiplied by the number of the particles in the inlet, $\dot{m}/m_{Ar}$, with m_{Ar} being the argon atomic mass. The ionisation energy is as follows

$$\dot{\varepsilon}_{ion} = \bar{Z}\varepsilon_1\frac{\dot{m}}{m_{Ar}} \tag{14}$$

where $\varepsilon_1 = 15.8$ eV is the ionisation energy of the groud level of an argon atom. Here only the first ionisation energy is used since $\bar{Z}$ in the inlet is less than 1.

The specific internal energy of the plasma at the inlet, $\dot{\varepsilon}_{int}$, is calculated using the IONMIX code. The excitation energy may be simply found by substracting the other two energies from $\dot{\varepsilon}_{int}$.

The efficiency is then

$$\eta = \frac{P_T}{P_M + P_\eta + \dot{\varepsilon}_{init}} = \frac{P_T}{UJ + \dot{\varepsilon}_{init}} \tag{15}$$

which now includes the energy losses related to the plasma inlet boundary conditions.

As discussed previously, in the high-power regime the thrust of an MPDT scales as J^2 while its power is expected to scales as J^4 (Andrenucci 2010). This trend is demonstrated in Fig. 4, which shows the total power calculated from the simulations as a function of current. In the high-power regime the work done per unit time by the Lorentz forces (shown in blue) dominates over ohmic heating (red), the latter is also responsible for the electrothermal acceleration of the propellant, which is negligible in this regime.

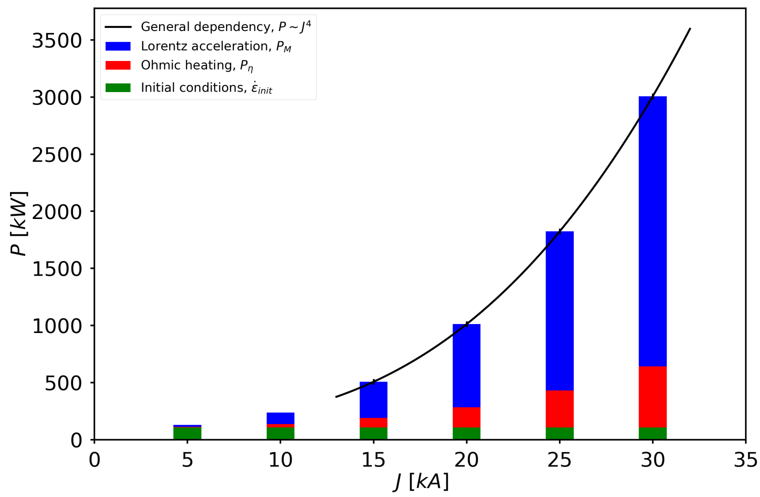

Figure 4: Power deposition and losses in the Villani MPDT setup. We show the power due to the Lorentz acceleration (blue), the ohmic heating (red) as well as the power spent to create the inlet plasma (green). The power losses due to the electrode sheaths are not considered here since they can not be modelled in the MHD approach, but can be roughly estimated from experimental data. The curve shows the expected $\sim J^4$ scaling which is valid at high currents.

The calculated efficiencies are found, see Table 3, to be 62% at 15 kA, 68% at 20 kA, 76% at 25 kA and 84% at 30 kA. The power associated with the injection of the plasma at the inlet, marked with green in Fig. 4, is negligible in the high-current regime. However in the low-current regime ($J \lesssim 10$ kA) it is responsible for most of the deposited power, therefore making the given inlet conditions rather inappropriate for this regime. By contributing to the cold thrust, these inlet conditions give unphysical efficiencies at low currents, resulting in 40% at 5 kA and 57% at 10 kA. Work is in progress to implement more realistic inlet conditions with relatively cold, weakly ionised plasmas for the low-current regime.

DOI: 10.13009/EUCASS2023-562

Table 1: Power deposition parameters

Driving current, J [kA]	Plasma voltage drop, U [V]	Power, UJ [kW]	Numerical efficiency, η [%]	Total efficiency, η_s [%]
5	4.5	22.5	49	19
10	13.2	131.7	57	20
15	26.7	400.8	62	26
20	45.3	905.3	68	35
25	68.7	1717.9	76	45
30	96.7	2900.7	84	56

The plasma voltage drop is deduced using Eq. 10.
See text for detailed description of the given parameters.

We also point out that the voltage drop associated with the electrode sheath is not included into the above calculations. However these can be roughly estimated using the anode voltage drop measurements done by Diamant 1996 for the PFSBT setup. For an anode voltage drop of ~50 V, the efficiencies would have to be revised to 19%, 20% 26%, 35%, 45%, 56% for the currents from 5 to 30 kA with 5 kA increment, see column η_s in Table 3.

4. Conclusions

We have presented resistive MHD simulations of the Villani MPDT setup performed with the FLASH code. The simulations reproduce the steady-state behaviour of the two well-known working regimes of MPDTs: electrothermal and electromagnetic. The calculated thrust values correlate well with appropriate theoretical predictions in both regimes. For the high-current regime the simulations are also capable of reproducing the general scaling of power with current $P \sim J^4$. We find that regions of low ionisation exist in the inter-electrode region at larger radii indicating that electron-neutral collisions should be taken into account in the modelling of the resistivity. Such work is in progress. Another valuable point is that the amount of power spent to generate the plasma conditions at the inlet of the simulations is inappropriate for the low-current regime. More suitable plasma inlet conditions, the means of their generation and computational difficulties that may arise are being investigated.

While the simulations can reproduce the correct dependence of the thrust and power on current, the geometry and physics considered in the model are unable to capture the onset. Future work will explore the importance of 3D effects as well as extended MHD physics on the ability of the model to capture the onset. Extension to 3D is of great importance in particular to capture non-axisymmetric MHD instabilities.

5. Acknowledgments

The authors acknowledges the Initiative "Physique des Infinis" of Sobonne Université for funding the doctoral thesis of YT. This project was granted access to the HPC resources of MesoPSL financed by the Region Ile de France and the project EquipMeso (reference ANR-10-EQPX29-01) of the programme Investissements d'Avenir supervised by the Agence Nationale pour la Recherche.

References

[1] Ahedo, E. "Plasmas for space propulsion". In: *Plasma Physics and Controlled Fusion* 53.12 (2011), p. 124037.

[2] Andrenucci, M. "Magnetoplasmadynamic thrusters". In: *Encyclopedia of Aerospace Engineering* (2010).

[3] Auweter-Kurtz, M. et al. "Numerical modeling of the flow discharge in MPD thrusters". In: *Journal of Propulsion and Power* 5.1 (1989), pp. 49–55.

[4] Boyle, M.; Clark, K., and Jahn, R. "Flowfield Characteristics and Perf ormance Limitations of Quasi-Steady Magnetoplasmadynamic Accelerators". In: *AIAA Journal* 14.7 (1976), pp. 955–962.

[5] Braginskii, S. "Transport processes in a plasma". In: *Reviews of plasma physics* 1 (1965), p. 205.

[6] Chelem Mayigué, C.; Kühn, C., and Groll, R. "Performance investigation of an argon fueled magnetoplasmadynamic thruster with applied magnetic field". In: *Journal of Applied Physics* 124.22 (2018), p. 223301.

DOI: 10.13009/EUCASS2023-562

[7] Choueiri, E. "Scaling of Thrust in Self-Field Magnetoplasmadynamic Thrusters". In: *Journal of Propulsion and Power* 14.5 (1998), pp. 744–753.

[8] Choueiri, E.; Kelly, A., and Jahn, R. "MPD thruster plasma instability studies". In: *19th International Electric Propulsion Conference*. 1987.

[9] Chung, H.-K.; Morgan, W., and Lee, R. "FLYCHK: an extension to the K-shell spectroscopy kinetics model FLY". In: *Journal of Quantitative Spectroscopy and Radiative Transfer* 81.1-4 (2003), pp. 107–115.

[10] Chung, H.-K. et al. "FLYCHK: Generalized population kinetics and spectral model for rapid spectroscopic analysis for all elements". In: *High energy density physics* 1.1 (2005), pp. 3–12.

[11] Diamant, K. D. *The anode fall in a high power pulsed MPD thruster*. Princeton University, 1996.

[12] *FLASH user's guide*. URL: `https://flash.rochester.edu/site/flashcode/user_support/flash4_ug_4p7.pdf`.

[13] Fryxell, B. et al. "FLASH: An adaptive mesh hydrodynamics code for modeling astrophysical thermonuclear flashes". In: *The Astrophysical Journal Supplement Series* 131.1 (2000), p. 273.

[14] Jahn, R. and Lyman, F. "Physics of Electric Propulsion. McGraw-Hill". In: *New York City* (1968).

[15] Kawasaki, A. et al. "MHD and Thermal Coupled Simulation of an MPD Thruster". In: *51st AIAA/SAE/ASEE Joint Propulsion Conference*. 2015, p. 3727.

[16] Kawasaki, A. et al. "MHD Simulation and Thermal Design of an MPD Thruster". In: *TRANSACTIONS OF THE JAPAN SOCIETY FOR AERONAUTICAL AND SPACE SCIENCES, AEROSPACE TECHNOLOGY JAPAN* 12 (2014), Pb_19–Pb_25.

[17] LaPointe, M. and Mikellides, P. "High power MPD thruster development at the NASA Glenn Research Center". In: *37th Joint Propulsion Conference and Exhibit*. Joint Propulsion Conferences. American Institute of Aeronautics and Astronautics, 2001.

[18] Macfarlane, J. J. "IONMIX - a code for computing the equation of state and radiative properties of LTE and non-LTE plasmas". In: *Computer Physics Communications* 56.2 (1989), pp. 259–278.

[19] Maecker, H. "Plasmaströmungen in Lichtbögen infolge eigenmagnetischer Kompression". In: *Zeitschrift für Physik* 141.1 (Feb. 1, 1955), pp. 198–216.

[20] Mazouffre, S. "Electric propulsion for satellites and spacecraft: established technologies and novel approaches". In: *Plasma Sources Science and Technology* 25.3 (2016), p. 033002.

[21] Randolph, T. et al. "Measurement of ionization levels in the interelectrode region of an MPD thruster". In: *28th Joint Propulsion Conference and Exhibit*. 1992, p. 3460.

[22] Sankaran, K.; Jardin, S., and Choueiri, E. "Parallelization and validation of an MHD code for the simulation of self-field MPDT flows". In: *Proceedings of the 27th International Electric Propulsion Conference*. 2001.

[23] Sankaran, K.; Choueiri, E., and Jardin, S. "Comparison of simulated magnetoplasmadynamic thruster flowfields to experimental measurements". In: *Journal of propulsion and power* 21.1 (2005), pp. 129–138.

[24] Sankaran, K. "Simulation of MPD flows using a flux-limited numerical method for the MHD equations". PhD thesis. Citeseer, 2001.

[25] Sankaran, K. *Simulation of plasma flows in self-field Lorentz force accelerators*. Princeton University, 2005.

[26] Sutton, G. P. and Biblarz, O. *Rocket propulsion elements*. John Wiley & Sons, 2016.

[27] Tang, H.-B. et al. "Study of applied magnetic field magnetoplasmadynamic thrusters with particle-in-cell and Monte Carlo collision. II. Investigation of acceleration mechanisms". In: *Physics of Plasmas* 19.7 (2012), p. 073108.

[28] Tikhonov, V. et al. "Research of plasma acceleration processes in self-field and applied magnetic field thrusters". In: *Proc. 23rd International Electric Propulsion Conference*. 1993.

[29] Uribarri, L. *Onset voltage hash and anode spots in quasi-steady magnetoplasmadynamic thrusters*. Princeton University, 2008.

[30] Uribarri, L. and Choueiri, E. Y. "The onset of voltage hash and its relationship to anode spots in magnetoplasmadynamic thrusters". In: *29th International Electric Propulsion Conference*. 2005, pp. 2005–084.

[31] Villani, D. D. *Energy loss mechanisms in a magnetoplasmadynamic arcjet*. Princeton University, 1982.

[32] Xisto, C. M.; Páscoa, J. C., and Oliveira, P. J. "Numerical analysis of real gas MHD flow on two-dimensional self-field MPD thrusters". In: *Acta Astronautica* 112 (2015), pp. 89–101.